Research Square

Preprints are preliminary reports that have not undergone peer review.
They should not be considered conclusive, used to inform clinical practice,
or referenced by the media as validated information.

Crystalline SiO2 modulates molecular hydrogen storage and redistribution in the Earth's interior

Luca Toffolo

luca.toffolo@uca.fr

Laboratoire Magmas et Volcans, Université Clermont-Auvergne https://orcid.org/0000-0001-8598-574X

Simone Tumiati

University of Milan https://orcid.org/0000-0003-0900-6145

Giorgia Confortini

École Normale Superiéure de Lyon https://orcid.org/0009-0000-8616-8282

Diego Gatta

Universita' degli Studi di Milano

Stefano Poli

Università degli Studi di Milano https://orcid.org/0000-0001-5313-1678

Anne-Sophie Bouvier

University of Lausanne https://orcid.org/0000-0002-5202-603X

Patrizia Fumagalli

Article

Keywords:

Posted Date: November 20th, 2026

DOI: https://doi.org/10.21203/rs.3.rs-11635233/v1

License: This work is licensed under a Creative Commons Attribution 4.0 International License.
Read Full License

Additional Declarations: There is **NO** Competing Interest.

Crystalline SiO_2 modulates molecular hydrogen storage and redistribution in the Earth's interior

Luca Toffolo[1,2], Simone Tumiati[1], Giorgia Confortini[3], G. Diego Gatta[1], Stefano Poli[1] , Anne-Sophie Bouvier[4], and Patrizia Fumagalli[1]

[1]DiSTAD, University of Milan, Milan, Italy.

[2]Laboratorie Magmas et Volcans, Clermont-Ferrand, France.

[3]LGL-TPE, École Normale Superiéure de Lyon, Lyon, France.

[4]Université de Lausanne (UNIL), Lausanne, Switzerland.

Corresponding author: Luca Toffolo (luca.toffolo@uca.fr)

Key Points:

- Experiments show that quartz and coesite can store large amounts of H_2 by intracrystalline physisorption at subduction-zone P–T–fO_2 conditions
- H_2 is stored within structural cavities and the uptake is proportional to the hydrogen chemical potential
- Evolving P–T–fO_2 conditions may trigger H_2 release from crystals, altering local redox conditions and deep hydrogen cycling.

Abstract

Molecular hydrogen (H_2) is increasingly recognized as an important volatile species in Earth's interior, yet the mechanisms governing its storage and transport remain poorly understood. Using high-pressure experiments performed under subduction-zone conditions (1.5–9.6 GPa, 500–950 °C) with externally buffered aqueous fluids (ΔFMQ ≈ −6.0 to +0.4) and analysis of the quenched fluids, we show that crystalline SiO_2 incorporates molecular H_2 through intracrystalline physisorption within its intrinsic structural voids. The equilibrium H_2 uptake is controlled by hydrogen chemical potential and reaches up to ~3000 μg H_2 g^{-1} SiO_2 in quartz. Changes in pressure, temperature, redox state, fluid conditions, as well as phase transitions modify the equilibrium partitioning of H_2, promoting its storage or release as geological conditions evolve. Intracrystalline physisorption therefore provides a previously unrecognized mechanism that modulates molecular hydrogen redistribution and redox evolution in Earth's interior.

1. Introduction

Hydrogen exerts a disproportionate influence on Earth's mantle geochemistry and geodynamics, controlling melting reactions, element mobility, redox state and evolution, and rock rheology despite its generally low abundance (*e.g.*, Demouchy and Bolfan-Casanova, 2016; Karato, 2006; Keppler et al., 2024; Ohtani, 2021; Kasting et al. 1993; Regeneauer Lieb et al., 2001). Hydrogen at depth is traditionally assumed to reside almost exclusively as H_2O-rich fluids and structurally bound hydroxyl (OH^-) in hydrous and nominally anhydrous minerals (Demouchy and Bolfan-Casanova, 2016). However, increasing analytical and experimental evidence indicates that molecular hydrogen (H_2) can also be incorporated into upper-mantle and eclogitic minerals at concentrations comparable to those of hydroxyl (Demouchy and Bolfan-Casanova, 2016; Malaspina et al., 2023; Moine et al., 2020; Yang et al., 2016). These observations suggest that H_2 may constitute an important deep hydrogen reservoir, with potentially significant implications for mantle redox evolution and hydrogen budgets.

Subduction zones are the principal gateway for hydrogen transport into the upper mantle. Fluids released from devolatilizing slabs span a wide range of pressures, temperatures and redox conditions (Poli et al., 2009; Cannaò and Malaspina, 2018; Caurant et al., 2023), allowing H_2 to become a major fluid species under reducing conditions, particularly during serpentinization of peridotitic protoliths (Evans et al., 2017; Vitale Brovarone et al., 2017, 2026; Merdith et al., 2023). As these fluids migrate through the slab and into the overlying mantle wedge they inevitably interact with common rock-forming minerals. Understanding how H_2 is transferred from fluids to silicates is therefore central to quantifying the deep hydrogen cycle.

Yet the physical process by which H_2 enters and is retained within silicates remains poorly understood. Unlike hydroxyl incorporation, which proceeds through protonation in structural defects, H_2 is electrically neutral and is therefore expected to interact with mineral structures through fundamentally different mechanisms. Among common rock-forming minerals, crystalline SiO_2 polymorphs provide a particularly suitable system for investigating this problem. Although generally regarded as essentially non-porous solids, quartz has long been known to be permeable to H_2 on experimental timescales (Mavrogenes and Bodnar, 1994; Hall and Sterner, 1995), while molecular dynamics simulations identify interconnected structural channels in quartz, coesite, and stishovite as preferential migration pathways for neutral gas species,

including H_2, under pressure-temperature conditions relevant to Earth's interior (Futera et al., 2017; Figowy et al., 2024). Likewise, high-pressure experiments demonstrate that silica glass and cristobalite can incorporate unexpectedly large amounts of H_2 within intrinsic structural voids (Efimchenko et al., 2013, 2014). Cristobalite, for example, accommodates up to 0.12 mol H_2 mol^{-1} SiO_2 at ~7.5 GPa and 250 °C, while most of the incorporated H_2 is released at room temperature after decompression (Efimchenko et al., 2014). Collectively, these independent observations support a mechanism in which H_2 migrates through an interconnected network of structural voids and is transiently stabilized by weak host-guest interactions rather than by the formation of chemical bonds.

Here we investigate the interaction between molecular H_2 and crystalline SiO_2 by equilibrating silica polymorphs with redox-buffered H_2–H_2O aqueous fluids over a wide range of pressures (1.5–9.6 GPa), temperatures (500–950 °C), and redox states (ΔFMQ ≈ –6.0 to +0.4). Most experiments were performed on quartz, with complementary runs spanning the quartz–coesite and coesite–stishovite transitions (see Methods; Supplementary Table 1). By comparing measured fluid compositions with thermodynamic predictions, we demonstrate that systematic deviations from the expected H_2–H_2O equilibrium are best explained by H_2 incorporation into crystalline SiO_2 during high-pressure equilibration, followed by its release during quenching and decompression. We then quantify the effects of pressure, temperature, and redox state on H_2 uptake and test whether the observed behavior is consistent with intracrystalline physisorption. Our results establish crystalline SiO_2 as a transient reservoir for molecular hydrogen and provide a mechanistic framework for understanding H_2 exchange between aqueous fluids and crystalline solids. More broadly, they suggest that intracrystalline physisorption may represent a previously unrecognized mechanism for transient hydrogen storage in nominally non-porous silicates, with implications for hydrogen transport, volatile cycling, and mantle redox evolution.

Results and Discussion

H_2 excess in quenched fluids

In all experiments, the quenched fluids coexisting with crystalline SiO_2 consist predominantly of H_2O–H_2 mixtures (Supplementary Table 2). However, the measured H_2 contents do not always match thermodynamic predictions. Instead, systematic H_2 excess develops toward higher pressures, lower temperatures, and increasingly reducing conditions (Fig. 1).

The pressure series provides the clearest illustration of this behavior. At 700 °C and WM-buffered conditions, measured H_2 content increases from ~3.5 µmol at 1.5 GPa to ~15 µmol at 2.8 GPa before decreasing slightly to ~12 µmol within the coesite stability field at 3 GPa (Fig. 1a). Agreement between measured and predicted values is observed at 1.5 GPa, whereas progressively larger discrepancies develop above ~2 GPa. A similar excess persists across the coesite–stishovite transition at 950 °C, where measured H_2 contents exceed thermodynamic predictions by three orders of magnitude at both 7.5 and 9.6 GPa (~3.1 and ~0.48 µmol vs. $6 \cdot 10^{-3}$ and $5 \cdot 10^{-4}$ µmol, respectively; Fig. 1b).

Systematic trends are equally evident in the temperature and redox series. At constant pressure (2 GPa) and WM-buffered conditions, the H_2 content decreases gradually from ~12 µmol at 500 °C to ~2 µmol at 900 °C, while the discrepancy between measured and predicted values progressively disappears toward the highest temperature investigated (Fig. 1c). At constant

pressure and temperature (2 GPa, 700 °C), H_2 remains below detection under the oxidizing FsMQ buffer, whereas it increases toward more reducing conditions, reaching ~26 µmol under IW-buffer (Fig. 1d). Molecular hydrogen excess increases systematically with decreasing oxygen fugacity. Together, the pressure, temperature, and redox state trends reveal that the magnitude of H_2 excess scales with the hydrogen fugacity of the coexisting aqueous fluid.

Two blank experiments, containing only the WM buffer assemblage in both the capsules, were carried out at 2 GPa and 700 °C. Both yielded H_2 abundances close to model predictions (~1.9 and ~1.5 µmol versus ~2.4 and ~1.7 µmol, respectively; Supplementary Table 1, Supplementary Table 2), demonstrating that the thermodynamic model well reproduce H_2 generation by the buffer assemblage (with discrepancies in the order of 10^{-1} µmol). Consequently, the observed H_2 excess, Δn_{H_2}, defined as the difference between measured and predicted H_2 values,

$$\Delta n_{H_2}\ (\mu mol) = n_{H_2,measured}\ (\mu mol) - \frac{X_{H_2,calculated} \cdot n_{H_2O,measured}(\mu mol)}{1 - X_{H_2,calculated}}$$

is specifically associated with the presence of crystalline SiO_2, rather than with the experimental assembly. This interpretation is further supported by the fact that the redox conditions imposed by our experimental assemblies, composed of a graphite heater and MgO sleeve, are comparable to or more oxidizing than Ni–NiO (Matjuschkin et al., 2015), hence significant hydrogen release is considered unlikely.

The most compelling evidence that the H_2 excess originates from the interaction with crystalline SiO_2 is provided by the experiments containing variable masses of quartz. At constant pressure, temperature, and redox conditions (2 GPa, 700 °C, WM-buffered), increasing the amount of quartz loaded into the capsule from 7 to 31 mg causes a progressive increase of the H_2 content of the quenched fluid from ~5.2 to 10.1 µmol (Supplementary Table 2; Fig. 1d), and the corresponding excess H_2 shows an approximately linear trend with the amount of SiO_2 present (Fig. 2). The approximately linear relationship demonstrates that H_2 excess is directly

proportional to the amount of crystalline SiO_2 present, indicating that it originates from the solid phase rather than from the fluid alone.

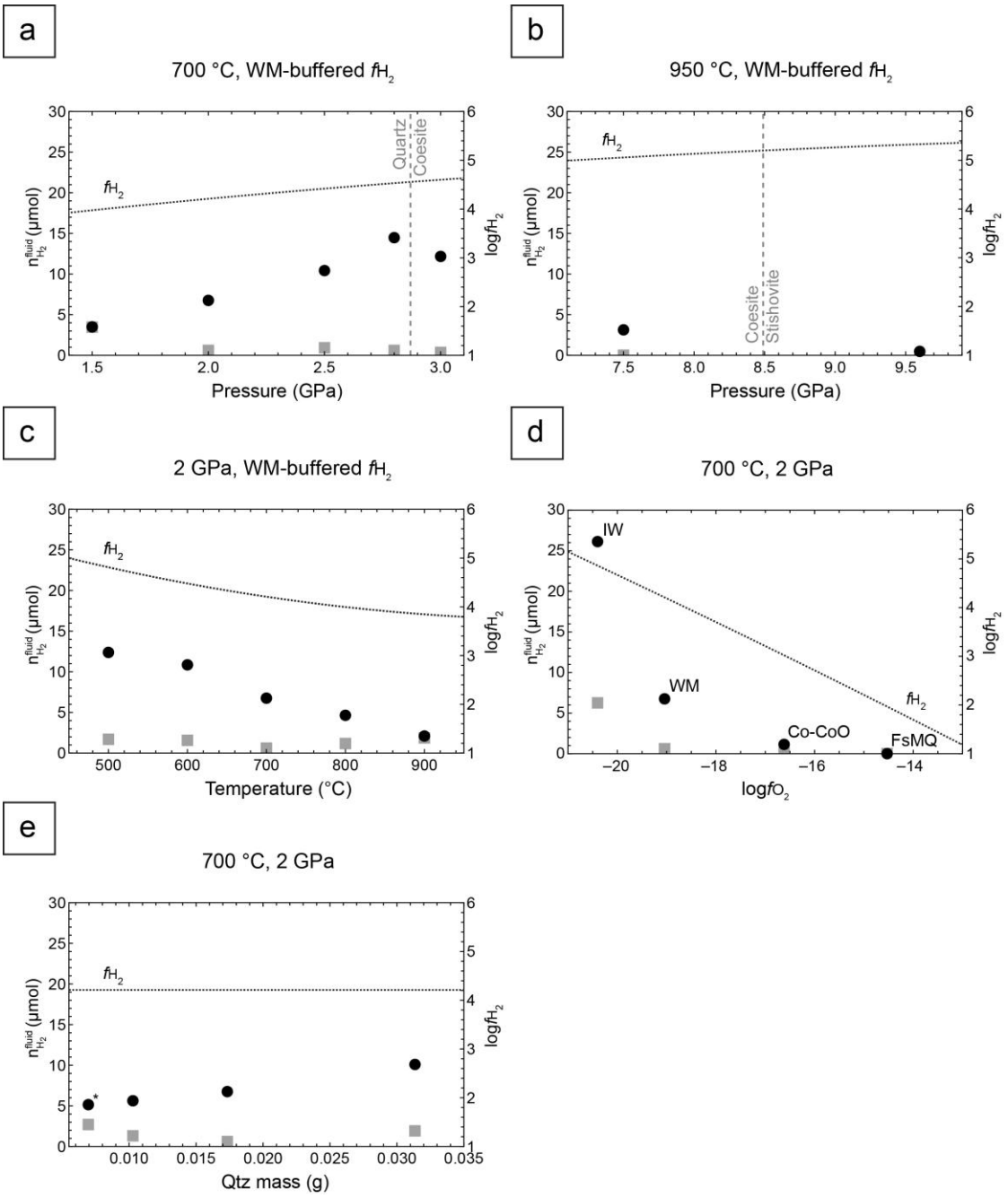


Figure 1. Measured hydrogen contents (black dots) in the fluid coexisting with crystalline SiO_2 and calculated hydrogen contents (grey squares) for the model SiO_2-free H–O system as a function of (a) pressure (700 °C, fH_2^{WM}), (b) progression through the coesite–stishovite transition (950 °C, fH_2^{WM}), (c) temperature (2 GPa, fH_2^{WM}), (d) redox state fixed by the buffer, expressed as logfO_2 (2 GPa, 700 °C), and (e) mass of quartz mass in the inner capsule (2 GPa, 700 °C, fH_2^{WM}). The asterisk in panel (e) denotes the single-crystal experiment. The fH_2 imposed by the buffer is also shown. Error bars are smaller than the symbols. Quartz-coesite and coesite-stishovite transition boundaries (dashed lines) are from Bose and Ganguly (1995) and Fei and Bertka (1999), respectively.

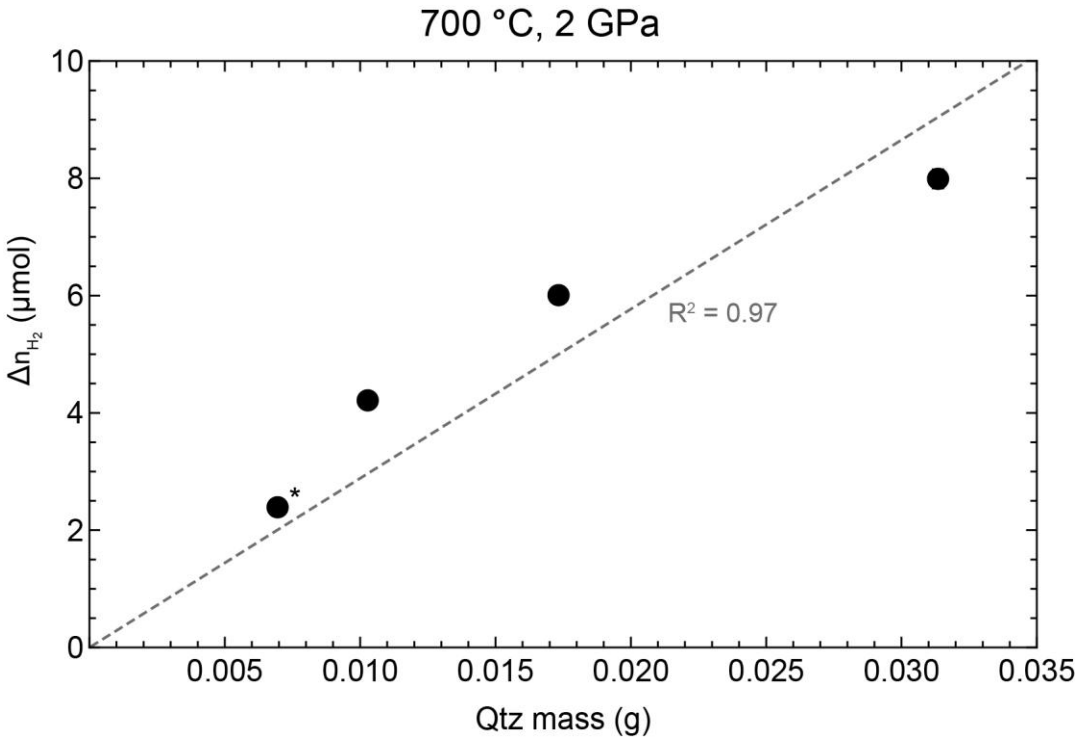


Figure 2. Excess H_2 (Δn_{H_2}) increases approximately linearly with quartz mass. The linear regression was constrained to pass through the origin because no excess H_2 is expected in the absence of quartz. The asterisk indicates the single-crystal experiment. Error bars are smaller than the symbol size.

H_2 incorporation through intracrystalline physisorption

The systematic dependence of H_2 excess on hydrogen fugacity, together with its proportionality to the mass of SiO_2, is characteristic of an equilibrium partitioning process between the solid and the coexisting fluid. A similar fugacity dependence has been documented for molecular hydrogen dissolution in silicate melts, where H_2 occupies the ionic porosity of the melt structure (Hirschmann et al., 2012). However, Raman spectroscopy of the recovered samples, together with the very low H/Si ratios measured by SIMS, indicates that even if quartz re-equilibrated with the experimental H_2-rich fluid, a negligible amount of H_2 is retained within the structure at room conditions (Fig. S1, Supplementary Table 3). This apparent contradiction is resolved if H_2 is incorporated only under run conditions and is subsequently redistributed back to the coexisting fluid during quenching and decompression, prior to sample recovery. An analogous behavior has been reported for cristobalite, in which H_2 incorporated at high pressure and detected by Raman spectroscopy of the samples quenched to –196 °C, is extensively released during a controlled ~10 min heating ramp to room temperature (Efimchenko et al., 2014).

The simplest interpretation is therefore that molecular H_2 enters an interconnected network of intrinsic structural voids, where it is transiently stabilized by weak host–guest interactions, i.e., intracrystalline physisorption. The nearly identical $\Delta n_{H_2}/SiO_2$ molar ratios (~0.021; obtained for both experiments containing powdered and single-crystal quartz (Supplementary Table 2), despite the vastly different specific surface areas involved, demonstrates that H_2 incorporation occur primarily within the crystal volume rather than on

external surfaces. This behavior is well documented in open-framework silicates such as zeolites, where gas molecules, including H_2, are incorporated through physisorption within structural channels and cages, with uptake increasing with pressure and decreasing with temperature (e.g., Feng et al., 2020). Our results indicate that the similar host-guest interactions may extend to the intrinsic sub-nanometric structural voids of crystalline SiO_2, despite the much stronger geometric confinement.

This is consistent with the crystal structures of the SiO_2 polymorphs and molecular dynamics studies on hydrogen diffusion. Quartz contains nominally empty [0001] channels formed by regular 6-membered rings of tetrahedra (free diameters ~2.2–2.3 Å, where "free diameter" of a cavity in a crystalline structure is defined as the effective internal aperture size calculated by subtracting twice the oxygen van der Waals radius (1.35 Å) from the oxygen-oxygen interatomic distances, across the ring opening; Baerlocher et al., 2007), together with distorted 6-membered rings along [01–10] (~3.3 × 2.2 Å) (Fig. 3a), both geometrically large enough to accommodate H_2 molecules (approximate size 1.2 × 2.2 Å). Likewise, coesite contains elliptical channels, confined by 6-membered rings of tetrahedra, along [001] (free diameters ~4.8 x 1.6 Å) that are also potentially capable of hosting H_2 (Fig. 3b). Simulations of atomic hydrogen identify channels parallel to the *c*-axis of α-quartz as energetically favorable migration pathways (Bongiorno et al., 1997), whereas simulations of molecular hydrogen demonstrate diffusion through the same interconnected channel network under pressure–temperature conditions relevant to Earth's interior (Futera et al., 2017).

Further support for structural control is provided by the coesite–stishovite transition. Whereas quartz and coesite exhibit comparable H_2 uptake despite their distinct crystal structures, the transition to stishovite is accompanied by an abrupt decrease in H_2 uptake, from ~0.014 to ~0.003 mol H_2 mol^{-1} SiO_2. In contrast to the tetrahedral frameworks of quartz and coesite, the rutile-type structure of stishovite contains substantially narrower [001] cavities (free diameters ~1.7 × 1.7 Å) confined by corner-sharing octahedra (Fig. 3c), markedly reducing the volume available for molecular hydrogen while remaining accessible to smaller noble gas atoms, such as He and Ne (Figowy et al., 2024).

Alternative explanations fail to account for experimental observations. The nearly linear relationship between Δn_{H_2} and SiO_2 mass excludes the possibility that H_2 excess originates from an unidentified dissolved species unstable at ambient conditions (e.g., silanes), which would instead produce comparable H_2 concentrations regardless of the amount of quartz present (contrarily, in the four variable-mass experiments H_2 concentrations range between 4 and 17 mol%). Likewise, the observed trends cannot be related to silica solubility and the reduction of H_2O activity that accompany aqueous silica formation. Although dissolved silica concentrations increase strongly with temperature, reaching up to ~4 molal at 900 °C and 2 GPa (Manning, 1994), the largest H_2 excesses are observed at lowest temperatures, whereas H_2 excess disappears under conditions where silica solubility is greatest. Consistent with the experiments of Manning (1994), the highest dissolved silica concentrations in our experiments are indicated by abundant sub-micrometric spheres of amorphous silica in the quenched fluid from the 900 °C experiment (Fig. S2, Fig. S3). Furthermore, because all experiments were performed under quartz- or coesite-saturated conditions, changing the amount of crystalline SiO_2 at constant pressure, temperature

and redox state does not modify dissolved silica concentrations and therefore cannot account for the observed dependence of H_2 excess on SiO_2 mass.

Taken together, these lines of evidence –including the dependence of H_2 uptake on hydrogen fugacity, its proportionality to the amount of crystalline SiO_2, the crystal-structure constraints, the molecular dynamics simulations, and the abrupt decrease in uptake across the coesite–stishovite transition– provide mutually consistent evidence that transient H_2 incorporation occurs through intracrystalline physisorption.

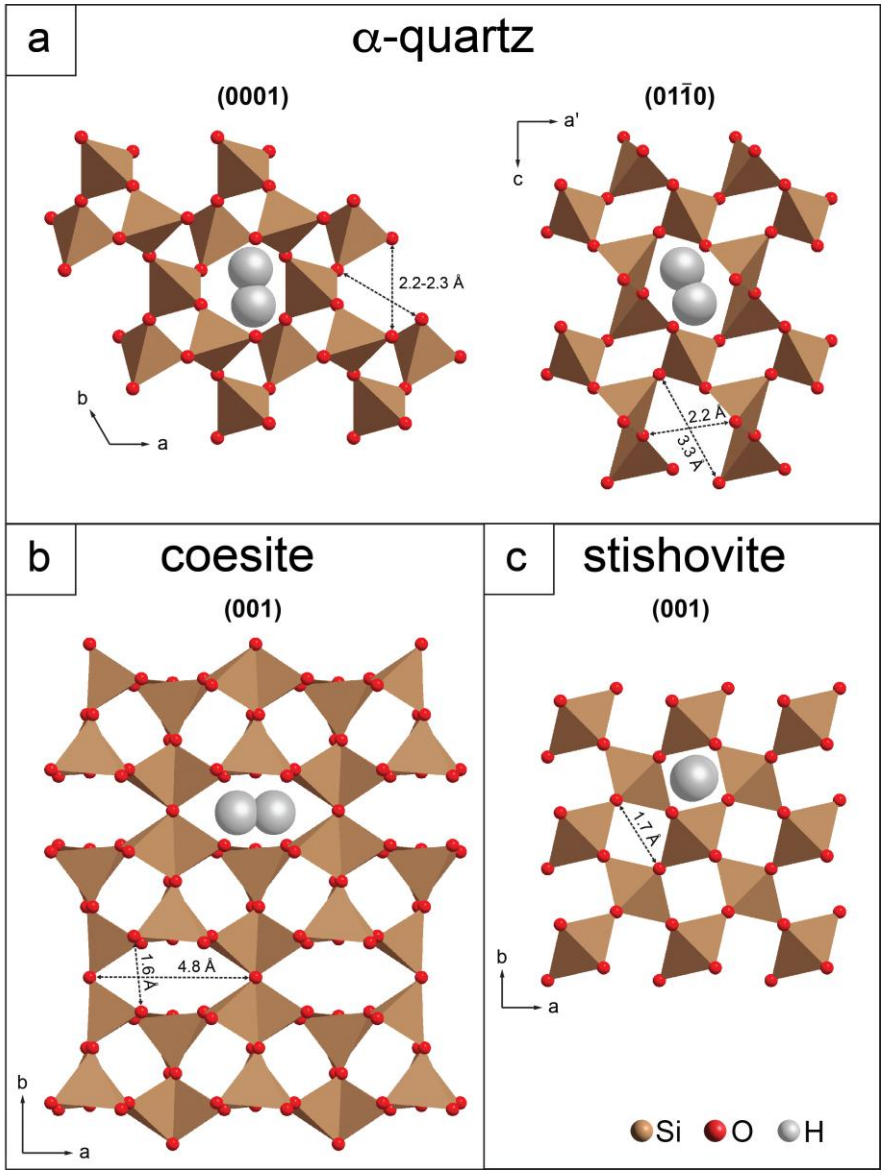


Figure 3. Potential environments for molecular hydrogen incorporation in (a) α-quartz (left, view down the *c*-axis; right, view down the *b*-axis), (b) coesite (view down the *c*-axis), and (c) stishovite (view down the *c*-axis). The markedly smaller structural cavities in stishovite are expected to impose stronger orientational constraints on H_2 molecules and may contribute to its lower H_2 uptake relative to quartz and coesite.

Pressure, temperature and redox controls on H_2 uptake

Normalizing Δn_{H_2} to the molar amount of crystalline SiO_2 isolates the intrinsic H_2 uptake capacity of the mineral (Supplementary Table 2):

$$n_{H_2}^{SiO_2} = \frac{\Delta n_{H_2}}{n_{SiO_2}}$$

At 700 °C under WM-buffered conditions, the normalized H_2 content increases rapidly with pressure before approaching a plateau of approximately 0.038–0.040 mol H_2 mol^{-1} SiO_2 above ~2.5 GPa (Fig. 4a). This asymptotic behavior is consistent with progressive occupation of a finite population of incorporation sites. Remarkably, the capacity remains essentially unchanged across the quartz–coesite transition (2.8–3.0 GPa), indicating that the structural reorganization accompanying the polymorphic transformation has little effect on the amount of H2 accommodated by crystalline SiO_2.

Temperature and redox state exert opposite effects on H_2 uptake. At constant pressure (2 GPa) and WM-buffered conditions, the normalized H_2 content decreases monotonically from ~0.034 mol H_2 mol^{-1} SiO_2 at 500 °C to ~0 at 900 °C (Fig. 4b). In contrast, progressively reducing conditions markedly enhances incorporation. At 2 GPa and 700 °C, the amount of incorporated H_2 increases from negligible values under FsMQ-buffered conditions to ~0.089 mol H_2 mol^{-1} SiO_2 at IW (Fig. 4c), corresponding to approximately 3000 µg H_2 g^{-1} SiO_2.

The magnitude of H_2 uptake is comparable to that reported for other silica frameworks. Cristobalite incorporates approximately 0.04 mol H_2 mol^{-1} SiO_2 at 250 °C under an hydrogen pressure of 2 GPa (Efimchenko et al., 2014), whereas silica glass incorporates comparable amounts of noble gases under pressure (~0.013–1.5 mol He mol^{-1} SiO_2 at 2 GPa; Sato et al., 2011), suggesting that occupation of intrinsic structural voids may be a general property of silica frameworks.

To quantitatively describe the experimental trends, the pressure-, temperature-, and redox- dependent datasets were fitted using logistic functions,

$$n_{H_2}^{SiO_2}\,(700\,°C, fH_2^{WM}) = \frac{0.0381893}{1+e^{-14.4991(P-1.98743)}}$$

$$n_{H_2}^{SiO_2}\,(2\,GPa, fH_2^{WM}) = \frac{0.0348717}{1+e^{0.0135293(T-723.708)}}$$

$$n_{H_2}^{SiO_2}\,(2\,GPa, 700°C) = \frac{0.0885955}{1+e^{-0.188222(fH_2-22.496)}}$$

which reproduce both the onset of measurable H_2 uptake and the progressive approach to saturation ($R^2 \approx 1$ for all datasets). The logistic form is entirely empirical and is not intended to imply a specific adsorption model; rather, it provides a convenient mathematical description of the observed behavior over the investigated experimental range. Under WM-buffered

conditions, the pressure and temperature relationships can be combined into a two-dimensional surface,

$$n_{H_2}^{SiO_2}(fH_2^{WM}) = -0.0205195 + \frac{0.0384959}{1+e^{0.012442(T-708.575)}} + \frac{0.0381893}{1+e^{-14.4991(P-1.98743)}}$$

which predicts H_2 uptake as a continuous function of pressure and temperature (Fig. 5). This relationship provides the quantitative framework used in the thermodynamic analysis presented below.

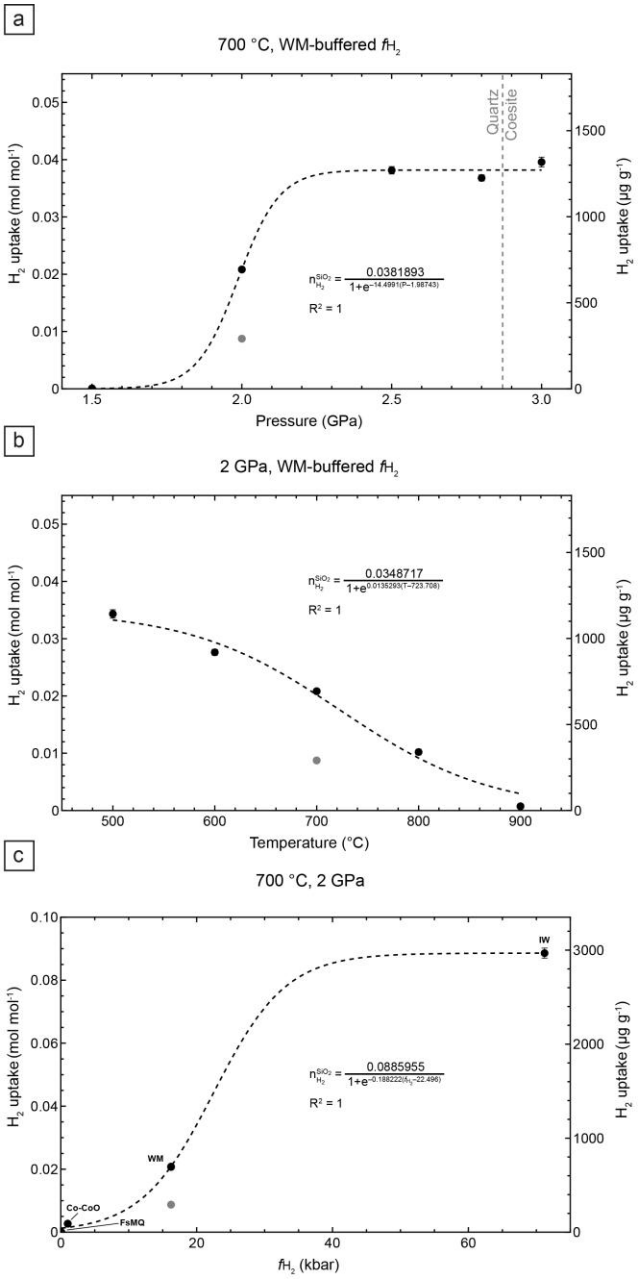


Figure 4. Molecular hydrogen uptake as a function of (a) pressure, (b) temperature, and (c) hydrogen fugacity imposed by the buffer. Fit curves (dashed lines) are shown with their equations.

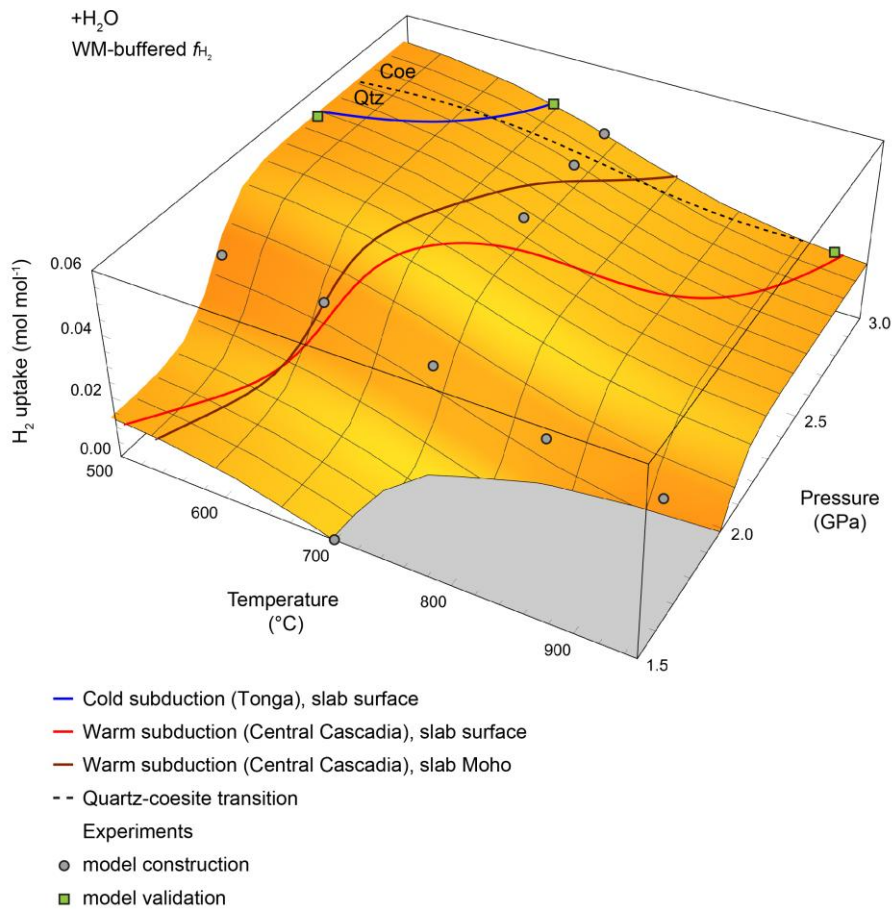


Figure 5. Empirical model describing H_2 uptake by crystalline SiO_2 as a function of pressure and temperature under WM-buffered conditions. Representative slab-surface and Moho geotherms for warm (Central Cascadia) and cold (Tonga) subduction zones are superimposed to illustrate the pressure–temperature conditions under which the model predicts H_2 uptake in subduction environments. The cold-subduction slab Moho geotherm is omitted because it lies largely outside the pressure range considered here. Grey circles denote the experimental data used to calibrate the model, whereas green squares indicate independent validation experiments. Slab geotherms are from Syracuse et al. (2010), and the quartz–coesite transition is from Bose and Ganguly (1995).

Thermodynamics of intracrystalline physisorption

The systematic dependence of H_2 uptake on pressure, temperature, and redox state strongly suggests that molecular hydrogen is incorporated through an equilibrium partitioning process governed by the coexisting H_2–H_2O fluid, with hydrogen chemical potential (itself a function of P, T and fH_2) acting as the thermodynamic driving force for H_2 incorporation into the crystal. A more rigorous test of the proposed mechanism is provided by its energetics. If H_2 is transiently stabilized within interconnected structural voids through intracrystalline physisorption, the associated differential enthalpy should be characteristic of weak host–guest interactions.

Because the experimental dataset samples only discrete pressure–temperature conditions, the differential enthalpy cannot be determined directly from the measurements.

Instead, uptake isotherms were generated by combining the empirical model described above with calculated equilibrium hydrogen fugacities (see Methods). Consequently, the calculated energetics should be regarded as model-dependent estimates that provide a thermodynamic consistency test of the proposed mechanism rather than direct experimental observables. Furthermore, because the interpolation is constrained primarily by experiments performed in the quartz stability field (with only one measurement available for coesite), the quantitative thermodynamic analysis formally applies to quartz. Nevertheless, the nearly identical uptake capacities measured across the quartz–coesite transition suggest that similar energetics are likely to characterize both polymorphs.

The differential enthalpy is negative over the entire investigated loading range, confirming that H_2 incorporation is an exothermic process (Fig. 6; Supplementary Table 4). It decreases from approximately −31 kJ mol^{-1} at low H_2 uptake (loading) to a broad minimum of −38 ± 2 kJ mol^{-1}, before becoming slightly less negative as saturation is approached. The corresponding enthalpy magnitude (~38 kJ mol^{-1}) is substantially smaller than values characteristic of chemisorption yet significantly larger than those commonly associated with conventional H_2 physisorption on open porous materials (cfr. Tedds et al., 2011). Such intermediate values are consistent with strongly confined physisorption**,** where the cumulative effect of multiple weak interactions between H_2 and the surrounding framework produces stronger stabilization than simple van der Waals adsorption, while remaining fundamentally distinct from chemical bond formation.

The dependence of the differential enthalpy on H_2 uptake provides additional insight into the incorporation mechanism. The progressively more negative enthalpy at low uptake suggests that increasing hydrogen fugacity promotes access to energetically more favorable regions of the interconnected channel network. A similar relationship between H_2 uptake, gas pressure, and pore geometry has been reported for zeolites, where H_2 uptake increases with H_2 pressure and is greatest in materials containing pores whose size is comparable to the molecular dimensions of H_2 (Yaremov and Il'in, 2008). This latter behavior has been attributed to the overlap of the attractive interaction potentials generated by opposing pore walls. An analogous effect may operate in quartz and coesite, where confinement within sub-nanometric structural voids allows molecular H_2 to experience the cumulative attractive interactions generated by the surrounding SiO_2 framework, resulting in stronger host–guest interactions while remaining stabilized exclusively by weak non-covalent forces. The slight increase in differential enthalpy observed as saturation is approached may reflect progressive occupation of less favorable intracrystalline environments once the most stable sites have been filled. However, this trend coincides with the region where the uptake isotherms become nearly horizontal, so that the hydrogen fugacity associated with a given H_2 uptake value is less well constrained, resulting in larger uncertainties in the calculated differential enthalpy. Overall, the uptake dependence of the differential enthalpy indicates that molecular hydrogen does not experience a single uniform energetic environment within crystalline SiO_2.

The thermodynamic constraints therefore support stabilization of molecular H_2 within the intrinsic structural voids of quartz by intracrystalline physisorption, thereby allowing crystalline

SiO_2 to behave as a transient H_2 reservoir at the pressure–temperature–redox conditions characteristic of the Earth's interior.

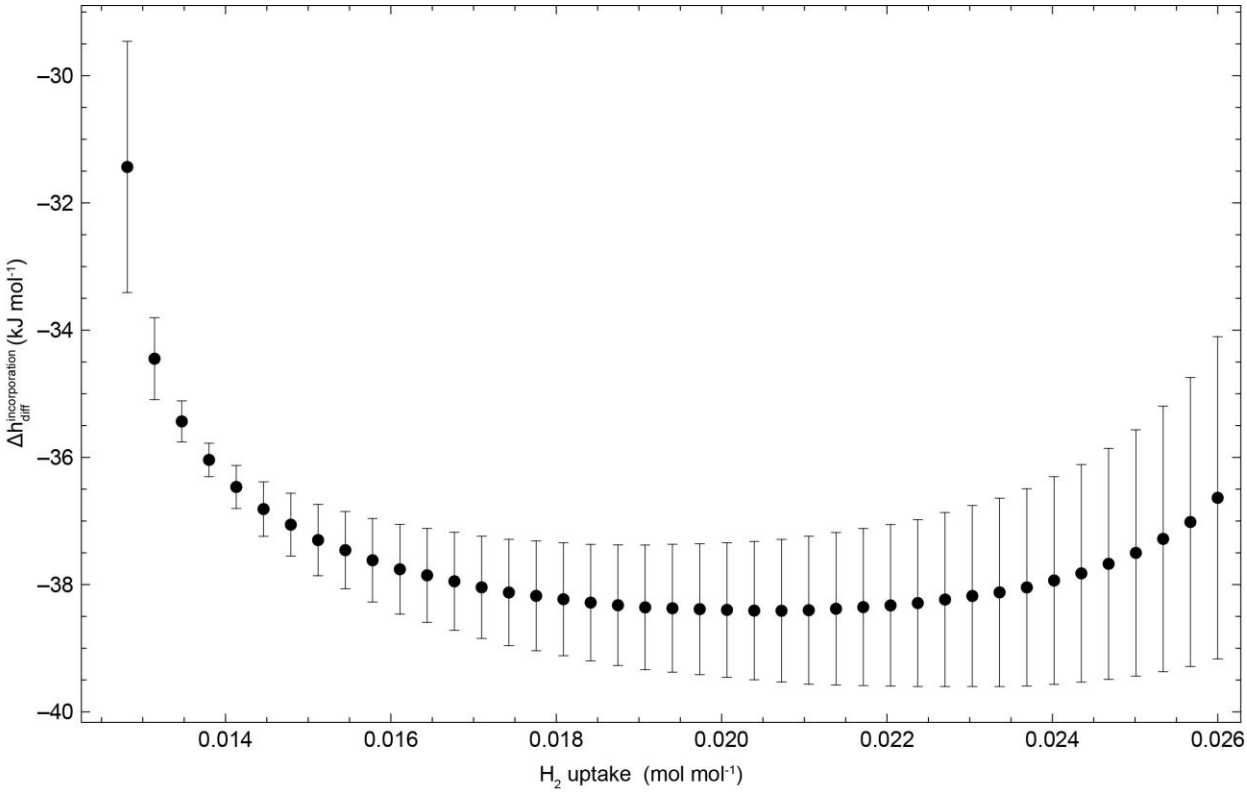


Figure 6. Differential enthalpy of H_2 incorporation as a function of H_2 uptake. Error bars represent ±1σ uncertainties derived from the linear regression of lnf_{H_2} versus 1/T at constant n. The uncertainty increases toward both low and high uptake because f_{H_2} varies only weakly with temperature under these conditions, making the regression less sensitive and hence the calculated differential enthalpy less constrained. The inset shows possible incorporation environments for H_2 molecule in quartz structure

Crystalline SiO_2 as a H_2 reservoir

The pressure–temperature conditions over which intracrystalline physisorption is observed closely overlap those encountered in subduction zones (Fig. 5). The slab surface, subduction channel, and overlying mantle wedge host aqueous fluids capable of sourcing H_2 (Schmidt and Poli, 2014). Because crystalline silica polymorphs are ubiquitous in subducted sediments, continental crust, and eclogitized oceanic crust –for example, through the reaction albite = jadeite + quartz–, a significant portion of the subducting slab may be involved in the process of H_2 incorporation.

The H_2 storage capacity of quartz is large, with maximum uptake reaching approximately 3000 μg g^{-1}, while coesite exhibits comparable capacities to at least 7.5 GPa, demonstrating that the storage mechanism remains effective well beyond the stability field of most hydrous minerals (≤3–6 GPa along slab surfaces; Keppler et al., 2024; Schmidt and Poli, 2014). By comparison, structurally bound hydrogen typically reported for natural quartz averages only ~1 μg H_2 equivalent g^{-1}, and rarely reaches ~30 μg g^{-1} (Stalder, 2021). Molecular H_2 should therefore be

considered alongside hydroxyl as a potentially important hydrogen species in crystalline silica under sufficiently reducing conditions.

Although the largest H_2 uptakes were obtained under WM-buffered conditions (ΔFMQ ≈ −2.5 to −5.9), measurable values persists over a substantially wider redox range. At 2 GPa and 700 °C, for example, quartz still incorporates ~100 μg g^{-1} H_2 under the more oxidizing Co–CoO buffer (ΔFMQ ≈ −1.6). Comparable or more reducing conditions are plausible in natural subduction environments, particularly during serpentinization and serpentinite dehydration (ΔFMQ ≈ −3; Evans et al., 2017; Debret and Sverjensky, 2017), and in carbon-saturated ultramafic lithologies where the EMOG/D (enstatite + magnesite–olivine + graphite/diamond) equilibrium approaches WM at depth. The redox state of slab-derived fluids is itself expected to be spatially heterogeneous because it depends on the extent of fluid–rock interaction and the degree of equilibration with the host lithology (Evans et al., 2013; Foley, 2011; Malaspina et al., 2017). These considerations indicate that the hydrogen fugacity required for significant H_2 uptake is not restricted to exceptionally reducing environments, but may develop locally wherever aqueous fluids interact with crystalline silica-bearing rocks. Consequently, intracrystalline physisorption may complement hydroxyl incorporation as an additional mechanism for hydrogen storage in subduction environments.

The empirical uptake relationships derived in this study provide a first-order framework for evaluating where intracrystalline physisorption is expected to be most effective. Extrapolation along representative slab geotherms predicts maximum H_2 storage at intermediate depths (<100 km), where temperatures remain sufficiently low to maintain favorable stabilization (Fig. 7). Additional experiments performed along warm and cold subduction geotherms closely reproduce the model predictions with a maximum relative error of ~16% (Supplementary Table 1; Supplementary Table 2; Fig. 5), supporting their applicability beyond the calibration dataset. Interestingly, the predicted maxima coincide with regions of extensive slab dehydration (Manning, 2004; Schmidt and Poli, 2014), where slab-derived aqueous fluids interact with silica-bearing lithologies. These suggest that intracrystalline physisorption may constitute a widespread mechanism governing equilibrium partitioning of molecular hydrogen between aqueous fluids and crystalline silica during subduction.

Even though the present study focuses on SiO_2 polymorphs, the underlying physical mechanism may extend to other common silicates. High-pressure H_2-loaded diamond-anvil cell experiments on forsterite revealed an anomalous lattice expansion accompanied by a shift of the H_2 vibron above ~3 GPa, both interpreted as evidence for molecular hydrogen incorporation (Shinozaki et al., 2012). Upon decompression at room temperature, the gradual recovery of the cell volume and disappearance of the H_2 vibron below ~2 GPa were attributed to loss of H_2 from the structure, consistent with a process of desorption. Although forsterite lacks the continuous channels present in quartz and coesite, small structural voids (triangular rings confined by corner-sharing octahedra or tetrahedra+octahedra with free diameters ranging between 1.5–2.1 Å) and/or crystallographic defects could provide pathways for H_2 migration. Therefore, these

observations raise the possibility that intracrystalline physisorption may represent a more general mechanism operating in nominally non-porous silicates.

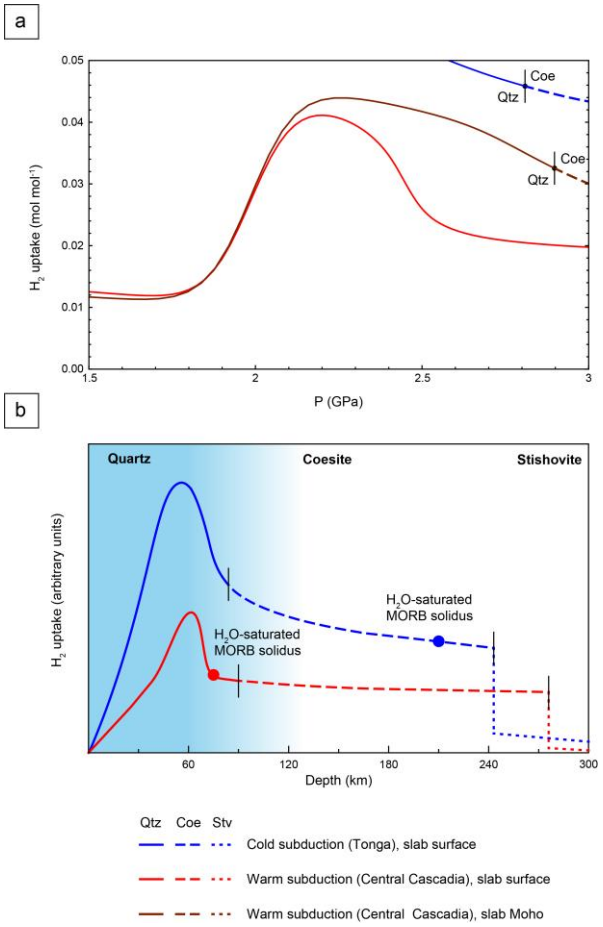


Figure 7. H_2 uptake along representative subduction paths. (a) Sections of the uptake surface from Fig. 5, cut along typical geotherms, reveal pronounced maxima in warm subduction zones. (b) Schematic relationship between H_2 uptake and depth along subduction zones, showing that a maximum is also expected for cold subduction settings, as uptake has to zero toward lowest pressures. The shaded area marks the approximate stability field of hydrous minerals. Vertical bars and dots indicate the approximate depths of SiO_2 phase transitions and intersections with H_2O-saturated MORB solidus curves, respectively. Abbreviations: Qtz = quartz; Coe = coesite; Stv = stishovite.

Redistribution of H_2 during subduction and implications for redox processes

Because intracrystalline physisorption represents an equilibrium partitioning process between crystalline silica and H_2-bearing fluids, the H_2 content of the crystal is controlled by the hydrogen chemical potential of the surrounding environment. In systems containing a finite hydrogen inventory, partitioning of H_2 into crystalline silica progressively decreases the H_2/H_2O ratio of the fluid until a new fluid–crystal equilibrium is established, thereby progressively shifting the residual fluid toward more oxidizing conditions. Conversely, where molecular hydrogen is continuously regenerated by ongoing fluid–rock reactions, the hydrogen fugacity remains buffered and the equilibrium H_2 content of crystalline silica is determined by the imposed

hydrogen chemical potential rather than by the cumulative amount of H_2 produced, as illustrated by the present experiments.

During subduction, changes in pressure, temperature, mineral assemblages, and fluid conditions continuously modify the equilibrium H_2 content of crystalline silica. Whether the crystal re-equilibrates with its surroundings depends on the kinetics of intracrystalline H_2 migration, which remain unconstrained under high-pressure conditions. The following discussion therefore explores the thermodynamic consequences of these evolving conditions, while recognizing that their realization in nature ultimately depends on the relative timescales of H_2 transport and geological processes.

As a slab sinks it experiences increasing pressures and temperatures. The empirical model predicts that H_2 uptake reaches a maximum at intermediate depths along both warm and cold slab geotherms (Fig. 7). Beyond this peak, continued increases in pressure and temperature progressively reduce the H_2 storage capacity of quartz and coesite. For example, along a warm Central Cascadia-type slab surface, increasing pressure from 2.2 to 2.5 GPa (corresponding to ~9–10 km sinking) decreases the predicted uptake from 0.041 to 0.026 mol H_2 mol^{-1} SiO_2, corresponding to the potential redistribution of approximately 500 g H_2 per metric ton of quartz. If sufficient time is available for re-equilibration, molecular hydrogen would progressively partition into surrounding grain boundaries, fluids, or melts. Alternatively, if intracrystalline diffusion is sluggish relative to geological timescales, part of the H_2 inventory may remain metastably retained.

Phase transitions may provide a particularly efficient mechanism for H_2 remobilization. Quartz and coesite exhibit similar uptake capacities despite their distinct crystal structures, whereas the transition to stishovite is accompanied by an abrupt decrease in H_2 equilibrium uptake associated with the collapse of the framework of tetrahedra. Along cold slab geotherms, where coesite transforms to stishovite at depths approaching 250–280 km, this structural reorganization may substantially reduce the equilibrium capacity for molecular hydrogen. Along a Tonga-type slab surface, coesite retains ~0.027 mol H_2 mol^{-1} SiO_2 immediately prior to transformation at ~8.2 GPa and ~790 °C, corresponding to the potential release of as much as ~900 g H_2 per metric ton of SiO_2.

The local equilibrium between crystalline silica and the coexisting fluid may be modified by migration of the fluid itself. If the carrier fluid is removed while pressure and temperature remain unchanged, the equilibrium H_2 content of crystalline silica becomes controlled by the hydrogen chemical potential established within the residual intergranular pore space rather than by the original fluid composition. Where H_2 released from crystalline silica accumulates within poorly connected grain boundaries or isolated pore volumes, the resulting increase in local hydrogen fugacity reduces the thermodynamic driving force for further release, allowing a significant fraction of the intracrystalline H_2 inventory to be retained. Conversely, efficient H_2 transport through interconnected fluid or fracture networks continually lowers the local hydrogen fugacity, promoting continued release from the crystal. The long-term preservation of molecular hydrogen in subduction environments is therefore expected to depend on the coupling between intracrystalline H_2 diffusion and intergranular H_2 transport, which together determine how rapidly local equilibrium can be re-established following fluid migration.

Release of molecular hydrogen from crystalline silica could generate fluids spanning a broad range of H_2/H_2O ratios, including extremely H_2-rich –and potentially even H_2-dominated–

fluid compositions. Such fluids constitute powerful reducing agents and have been invoked to explain reduction of carbon species to methane and graphite in shallow subduction environments, diamond formation at greater depths, stabilization of ultra-reduced phases such as moissanite, and the development of locally metal-saturated mantle domains (Boutier et al., 2021; Giuntoli et al., 2020, 2024; Ishimaru et al., 2009; Kepezhinskas et al., 2022; Peng et al., 2021, 2022; Stachel and Luth, 2015; Vitale Brovarone et al., 2017).

Partial melting is potentially capable of remobilizing molecular hydrogen. As H_2-bearing quartz or coesite are consumed during melting, a redistribution among residual solids, silicate melt, and any coexisting fluid will occur. Although the partitioning behavior of molecular hydrogen among these phases remains unconstrained, experiments indicate that H_2 solubility increases with melt polymerization, reaching up to ~0.9 wt% in andesitic melts at 2.5 GPa and 1400–1500 °C under IW-buffered conditions (Hirschmann et al., 2012). Silicate melts may therefore provide an efficient medium through which molecular hydrogen previously stored in crystalline silica is transferred throughout the mantle wedge.

The results presented suggest that, rather than constituting an additional source of H_2, intracrystalline physisorption in crystalline silica introduces an intermediate storage step into the deep hydrogen cycle. Molecular hydrogen generated by fluid–rock reactions may first be transiently sequestered within crystalline silica –and potentially within other silicates– and subsequently released as geological conditions evolve (Fig. 8). By partially decoupling the location of H_2 generation from its eventual participation in fluid-mediated redox reactions, intracrystalline physisorption may influence where and when reducing conditions develop within subduction zones. More broadly, intracrystalline physisorption reveals that molecular hydrogen can behave as a transient volatile component of common rock-forming minerals, introducing a previously unrecognized mechanism linking hydrogen transport, volatile cycling, and redox evolution in Earth's interior.

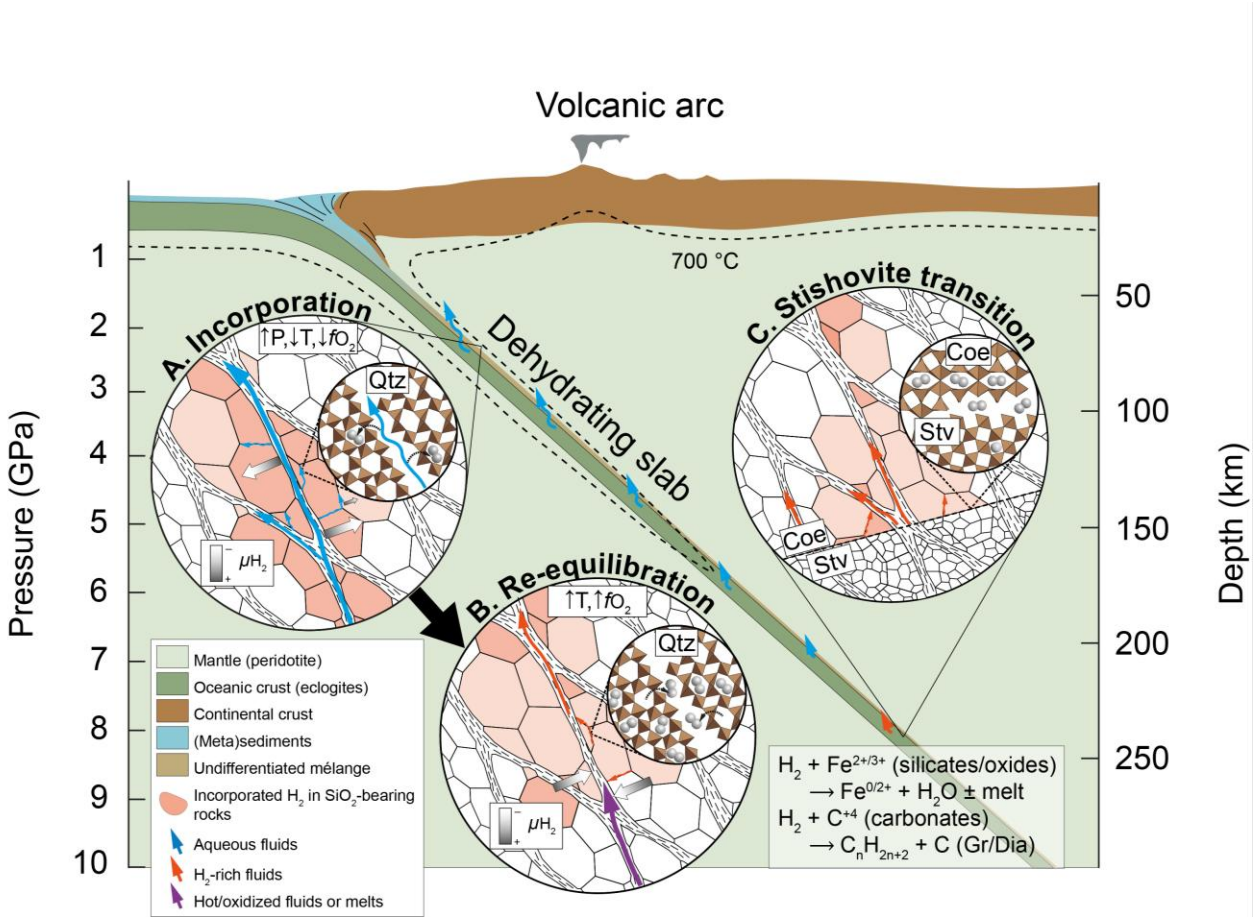


Figure 8. Schematic representation of molecular H_2 incorporation, transport, and redistribution in a simplified subduction-zone setting. (A) In the subducting crust and subduction channel, aqueous fluids of diverse origins and redox states percolate through quartz-bearing lithologies, including eclogites, metasediments, and underplated continental crust. Molecular hydrogen is transported through the system along gradients in hydrogen chemical potential (μH_2) and partitions between the fluid and crystalline silica, where it is incorporated through intracrystalline physisorption. The resulting H_2 uptake increases at higher pressures, lower temperatures, and more reducing conditions (low fO_2). (B) Progressive slab sinking and infiltration of hotter or more oxidized fluids or melts, perturb the equilibrium partitioning of molecular hydrogen by modifying the temperature, or the local hydrogen chemical potential. If re-equilibration occurs, H_2 may be released from crystalline silica and transferred to surrounding fluids or melts. (C) At greater depths, the coesite–stishovite transition, accompanied by densification of the crystal structure, may substantially reduce the equilibrium H_2 content of crystalline silica, inducing the release of part of the previously incorporated H_2. Migrating H_2 can participate in redox reactions involving oxidized Fe- and C-bearing species and phases, potentially contributing to the formation of H_2O, metallic alloys, hydrocarbons, graphite, or diamond.

Materials and Methods

Experimental strategy, capsule preparation, high-pressure apparatuses

The experiments were designed to determine whether crystalline SiO_2 polymorphs –primarily quartz, with comparison experiments in coesite and stishovite stability fields– can incorporate molecular hydrogen through adsorption under pressure–temperature–redox conditions representative of subduction zones (Supplementary Table 1). We used a classic double-capsule configuration (Eugster, 1957; Eugster and Skippen, 1967), where the inner capsule contains the SiO_2 charge and fluid, while the outer capsule hosts a solid-state redox buffer (Fig. S4). Hydrogen produced or consumed by the buffer diffuses through the capsule walls until a dynamic equilibrium is established, thereby imposing a controlled and homogeneous hydrogen fugacity (fH_2) on both capsules.

After each run, we quantified the volatile composition of the quenched fluid *ex situ*. The difference between the measured H_2 content in SiO_2-bearing experiments and that predicted from thermodynamic modeling of the buffer allowed us to determine the net amount of molecular hydrogen incorporated into the mineral at run conditions and released during quenching and decompression. Experiments were conducted between 1 and 9.6 GPa and 500–950 °C, using either a piston cylinder (1.5–3 GPa) or a multi-anvil apparatus (7.5–9.6 GPa) (Supplementary Table 2).

The experimental matrix systematically explored the effects of pressure, temperature, and redox state by varying one parameter at a time around a reference condition of 2 GPa, 700 °C, with fH_2 buffered by the wüstite–magnetite (WM) equilibrium. These experiments provided the foundation for an empirical model to predict H_2 bulk adsorption across a broader *P*–*T* range under WM-buffered conditions. Additional experiments addressed specific questions:

1) Assessing the mass dependency of the process, varying the amount of quartz loaded in the inner capsule while keeping all other variables fixed;
2) Evaluating volume/surface ratio effects, using a single euhedral quartz crystal instead of a polycrystalline sample;
3) Testing whether bulk H_2 adsorption extends to denser structures, investigating the coesite ($^{IV}SiO_2$)–stishovite ($^{VI}SiO_2$) transition;
4) Applying our findings to mantle lithologies, replacing quartz with forsterite.

Each experiment used ~20 mg of ultrapure quartz sand (≥99.995%, Sigma-Aldrich®) mixed with ~2 µL of ultrapure water (Milli-Q®), loaded into $Au_{60}Pd_{40}$ inner capsules (outer diameter, OD = 2.3 mm; inner diameter, ID = 2.0 mm). The quartz sand was calcined at 1000 °C for 1 hour to remove any incorporated H_2O (Dersch and Rauch, 1999; Doremus, 1995). A natural euhedral Herkimer quartz single crystal, free of visible inclusions (40× magnification), was used to test volume/surface ratio effects. Forsterite (Mg_2SiO_4) was synthesized by firing a pelletized stoichiometric mixture of nanocrystalline $Mg(OH)_2$ (99.9%, Sigma Aldrich®) and SiO_2 (99.9%, Balzers) at 1500 °C for 24 h. Blank experiments consisted of inner and outer capsules both filled with the redox-buffer assemblage.

AuPd capsules were inserted into larger $Au_{99.9}$ capsules (OD = 4.5 mm, ID = 4.1 mm in piston cylinder; OD = 3.0 mm, ID = 2.8 mm in multi-anvil experiments) along with water and the chosen redox-buffer assemblage. During the experiments, H_2 produced by buffer–water

reactions diffuses through the AuPd capsule walls, equalizing the fH_2 (or, equivalently, the hydrogen chemical potential) between inner and outer capsules and compensating for the possible loss of H_2 and H_2O to the assembly. Although water dissociation reaction links fH_2 to fO_2 (*e.g.*, Eugster and Wones, 1962; Shaw, 1963; Toffolo et al., 2023), equal fO_2 in both capsules requires identical fluid compositions, which is approximated but not guaranteed (*e.g.*, Boettcher et al., 1973; Miozzi and Tumiati, 2020). For this reason, we treat fH_2 as the primary imposed variable. Inner and outer capsules were welded while frozen using a gas tungsten arc welder (Lampert PUK U3), then leak-tested by weighing, immersion in ethanol under vacuum, and re-weighing. Any capsule showing mass changes was discarded.

Most experiments used a wüstite-magnetite (WM) fH_2 buffer:

$3FeO + H_2O \leftrightarrow Fe_3O_4 + H_2$, $\Delta FMQ \approx -2.4$ to -4.4

Additional buffers, used to explore the effect of redox state on H_2 incorporation at 700 °C and 2 GPa, include:

- Ferrosilite-magnetite-quartz (FsMQ)

  $3Fe_2Si_2O_6 + 2H_2O \leftrightarrow 2Fe_3O_4 + 6SiO_2 + 2H_2$, $\Delta FMQ \approx +0.4$

- Cobalt-cobalt oxide (Co–CoO)

  $Co + H_2O \leftrightarrow CoO + H_2$, $\Delta FMQ \approx -1.6$

- Iron-wüstite (IW):

  $Fe + H_2O \leftrightarrow FeO + H_2$, $\Delta FMQ \approx -5.7$

All buffer components (Fe, Co, FeO, Fe_3O_4, Co_3O_4, Fe_2O_3, amorphous silica) were reagent-grade Sigma-Aldrich® powders, with the exception of quartz that was obtained by grinding natural hyaline crystals. Fayalite was synthesized in a gas-mixing furnace from Fe_2O_3 and amorphous silica at 1100 °C under CO_2:CO = 10:1. Ferrosilite was generated *in situ* during experiments by reaction between fayalite and quartz. CoO was produced by heating Co_3O_4 at 1000 °C in flowing Ar and stored at 110 °C under vacuum to prevent re-oxidation. All powders were homogenized by grinding and checked for purity by X-ray powder diffraction.

Experiments in the quartz and coesite stability fields used a 600-ton rocking end-loaded piston cylinder apparatus (1.5 to 3 GPa) (Boyd and England, 1960). In this setup, the welded double capsule was positioned at the center of an assembly comprising an inner MgO rod, a graphite furnace, and an outer NaCl sleeve (acting as a pressure medium). For $T \geq 800$ °C, a Pyrex sleeve was interposed between the graphite furnace and the NaCl sleeve. A pyrophyllite-steel plug and lower graphite disk completed the electrical connection. Temperature was monitored with a K-type thermocouple (chromel–alumel; precision: ±5 °C), separated from the capsule by a 0.6 mm–thick Al_2O_3 disk. Under extremely reducing conditions (IW), a BN rod and AlN disk were used to avoid reaction with assembly materials. Pressure calibration followed the quartz–coesite phase transition (Bose and Ganguly, 1995) and its extrapolation to lower pressures for the end-loaded apparatus. Pressure uncertainty is ±0.01 GPa. Assemblies were compressed cold to target pressure, then heated at 100 °C/min. For runs at $T \geq 800$ °C, compression was paused at 0.25 GPa while heating to 400 °C to soften the Pyrex sleeve, after which final pressure and temperature

were reached. Experiments lasted for ≥6 h and quenching was achieved by power shutoff with water cooling, yielding cooling rates >40 °C/s.

One experiment in the stishovite stability field and one near the coesite-out boundary were conducted at 950 °C and pressures of 9.6 and 7.5 GPa, respectively, using a Walker-type multi-anvil apparatus (Walker et al., 1990). In this configuration, the load from a 1000-ton press was transmitted through six steel wedges to eight WC cubes (32 mm edges, 17 mm truncation), enclosing 25M MgO octahedra doped with 5 wt% Cr_2O_3. The double capsules were placed inside an MgO rod within a graphite furnace. Temperature was measured with an S-type thermocouple (±20 °C). Pressures were calibrated following Fumagalli and Poli (2005) with uncertainties of ±3%. Runs lasted 3 days and were quenched by power shutoff. The cooling rate is estimated to be similar to piston-cylinder experiments.

Analysis of fluids

After recovery, the outer Au capsules were opened and inspected for residual water in the buffer, providing a qualitative confirmation of its operation. The opened capsules were subsequently dried under vacuum at 110 °C to prevent residual buffer water from contaminating the fluid contained in the inner capsules. The inner capsules were analyzed using a capsule-piercing device coupled to a quadrupole mass spectrometer (QMS; Tiraboschi et al., 2016; Toffolo et al., 2025; Tumiati et al., 2017, 2020, 2022). Each capsule was loaded into a sealed Teflon chamber heated to approximately 90 °C. The chamber was flushed with Ar to remove atmospheric gases and adsorbed water, after which the capsule was pierced by advancing the capsule mount against a milling cutter. A high-sensitivity pressure gauge (±1 mbar) monitored the pressure change associated with gas release, and the liberated volatiles were transported by the Ar flow to the QMS through stainless-steel lines heated to 105 °C. An EXTORR XT 200 QMS equipped with a secondary electron multiplier simultaneously monitored 13 mass-to-charge (*m/z*) channels covering the principal fragmentation products of CH_4, CO, CO_2, H_2, H_2O, N_2, O_2. Each measurement lasted 1554 s. The resulting elution profiles were integrated and converted to micromoles using Mathematica® routines calibrated against standard gas mixtures. Analytical uncertainties were <1% for H_2O, CO_2, CH_4, and H_2, and ~10% for CO because of its overlap with N_2 at m/z = 28. Measurement accuracy was periodically verified by analyzing the products generated by the decomposition of oxalic acid dihydrate at 250 °C.

Analysis of solid phases

Following fluid extraction, samples were impregnated under vacuum with epoxy resin and prepared as standard 25.4 mm polished mounts. The preservation of the redox-buffer assemblages was verified using a JEOL 8200 wavelength-dispersive electron microprobe (15 kV, 5 nA, 1 µm beam; 30 s on-peak, 10 s background), using fayalite (Fe), grossular (Si), and metallic cobalt (Co) as standards.

SiO_2 polymorphs were identified using a Horiba LabRam HR Evolution ultra-low frequency Raman spectrometer with a 532 nm Nd:YAG laser and Peltier-cooled CCD. A 100× objective collected scattered light in backscattering geometry, with a 600 lines/mm grating and 100 µm hole. Calibration was performed before each set using a silicon wafer (main peak at 520.70 cm^{-1}).

Crystalline SiO_2 spectra were collected for 10 s with 3–4 accumulations using ~10 mW laser power, while the acquisition time was increased to 120 s to assess the presence of residual H_2.

Thermodynamic modeling

Oxygen and hydrogen fugacities (fO_2 and fH_2, respectively) and the equilibrium amount of H_2, were calculated for each redox buffer at the pressure-temperature conditions of the experiments (Supplementary Table 2). For the FsMQ, FMQ, and WM buffers, fO_2 was calculated using the CONVEX routine in Perple_X (v7.1.13; Connolly 1990, 2005) supported by the thermodynamic database of Holland and Powell (2011), integrated with thermochemical data for wüstite from Robie and Hemingway (1995). For the IW buffer, fO_2 was obtained following the parametrization of Hirschmann (2021), whereas, for the Co–CoO buffer, it was calculated using the formulation of Fegley (2013), which incorporates the thermodynamic data of O'Neill and Pownceby (1993). The corresponding fH_2 values and the equilibrium mole fraction of H_2 in the H–O fluid, XH_2,

$$X_{H_2} = \frac{n_{H_2}}{n_{H_2} + n_{H_2O}}$$

(where n_i is the amount, in moles, of the species H_2 or H_2O), were calculated using the FLUIDS routine in Perple_X and the hybrid modified Redlich–Kwong equation of state for the H–O system (PSEoS; Holloway, 1977; Connolly, 1995; Pitzer and Sterner, 1994). For each buffer, the fluid composition parameter X_O,

$$X_O = \frac{n_O}{n_H + n_O}$$

(where n_i denotes the amount, in moles, of either oxygen or hydrogen atoms) was varied until the calculated fluid fO_2 matched that imposed by the buffer. The resulting X_O, P and T values were then used as inputs to calculate fH_2 and XH_2. Finally, the equilibrium amount of H_2, $n_{H_2,calc}$, expected in each experiment was calculated from the measured amount of H_2O, $n_{H_2O,meas}$, as

$$n_{H_2,calc} = n_{H_2O,meas} \cdot \frac{X_{H_2,calc}}{1 - X_{H_2,calc}}$$

Thermodynamic analysis of H_2 uptake

Because the experimental dataset samples only discrete pressure–temperature conditions, the differential enthalpy cannot be obtained directly from the measurements. Instead, it was derived from continuous uptake isotherms generated using the empirical uptake model described above. Consequently, the calculated enthalpies should be regarded as model-dependent estimates that provide a thermodynamic test of the proposed mechanism rather than direct experimental observables.

The energetics of H_2 uptake were evaluated to independently assess whether the observed incorporation behavior is consistent with intracrystalline physisorption. Because H_2 uptake is inferred to occur within confined intracrystalline structural voids rather than on an external surface, we adopted the solution-thermodynamic treatment proposed by Myers (2002) for adsorption of multicomponent gas mixtures in microporous materials. In this framework, uptake is expressed as a function of hydrogen fugacity rather than total pressure, thereby avoiding the

ideal-gas approximation inherent to pressure-based treatments and relating H_2 uptake directly to the chemical potential of hydrogen.

The empirical pressure-, temperature-, and redox-dependent uptake relationships were combined with equilibrium hydrogen fugacities to generate H_2 uptake isotherms at 500, 600, 700, and 800 °C (Fig. S5). For each temperature, uptake was evaluated over a pressure range extending from the onset of measurable incorporation (~0.01 mol H_2 mol^{-1} SiO_2) to near saturation. The differential enthalpy associated with H_2 incorporation was then calculated from the Clausius–Clapeyron relation

$$\Delta h_{diff}^{incorporation} = -R\left(\frac{\partial ln f_{H_2}}{\partial(1/T)}\right)_{n_{H_2}^{SiO_2}}$$

where *R* is the universal gas constant, $ln f_{H_2}$ is the equilibrium hydrogen fugacity, *T* is the absolute temperature , and the derivative is evaluated along lines of constant H_2 uptake ($n_{H_2}^{SiO_2}$, in mol H_2 mol^{-1} SiO_2). The differential enthalpy was determined over the full range of measurable incorporation. This variable quantifies the energy change associated with incorporating an additional H_2 molecule into crystalline SiO_2 at constant H_2 loading. Its magnitude reflects the strength of the interaction between molecular hydrogen and the host framework, whereas its variation with H_2 uptake provides information on the energetic heterogeneity of the available incorporation sites. Together, these quantities provide an independent thermodynamic basis for assessing whether H_2 uptake is governed predominantly by weak host–guest interactions characteristic of physisorption or by the formation of stronger chemical bonds.

Acknowledgements

This research has been supported by the MIUR project “Dipartimenti di Eccellenza 2023–2027”.

Author contributions

L.T.: Writing – Original draft, Conceptualization, Methodology, Software, Validation, Formal analysis, Investigation, Data curation, Visualization; S.T.: Writing – Review and editing, Conceptualization, Methodology, Software, Validation, Formal analysis, Data curation, Resources, Project administration, Funding acquisition; G.C.: Writing – Review and editing, Investigation, Formal analysis; G.D.G: Writing – Review and editing, Formal analysis, Validation; S.P.: Writing – Review and editing, Validation, Resources, Project administration, Funding acquisition; A.-S.B.: Writing – Review and editing, Formal analysis, Investigation; P.F.: Writing – Review and editing, Formal analysis, Investigation, Resources, Project administration, Funding acquisition.

Data availability

The data supporting the findings of this study are available within the article, its Supplementary Information, and the Figshare repository at https://doi.org/10.6084/m9.figshare.34923636.

Code availability

The Mathematica® notebook used to process the mass spectrometry data is available in the Figshare repository at https://doi.org/10.6084/m9.figshare.34923636.

Conflict of Interest Disclosure

The authors declare there are no conflicts of interest for this manuscript.

References

Baerlocher, C., McCusker, L. B., and Olson, D. H. (2007). Atlas of zeolite framework types. Elsevier Science, 6th revised edition, Elsevier, Amsterdam.

Bongiorno, A., Colombo, L., and Cargnoni, F. (1997). Hydrogen diffusion in crystalline SiO_2. Chemical physics letters, 264, 435–440.

Boyd, F. R., and England, J. L. (1960). Apparatus for phase-equilibrium measurements at pressures up to 50 kilobars and temperatures up to 1750 °C. Journal of Geophysical Research, 65, 741–748.

Boettcher, A. L., Mysen, B. O., and Allen, J. C. (1973). Techniques for the control of water fugacity and oxygen fugacity for experimentation in solid-media high-pressure apparatus. Journal of Geophysical Research, 78, 5898–5901.

Bose, K., and Ganguly, J. (1995). Quartz-coesite transition revisited: reversed experimental determination at 500–1200 °C and retrieved thermochemical properties. American Mineralogist, 80, 231–238.

Boutier, A., Vitale Brovarone, A., Martinez, I., Sissmann, O., and Mana, S. (2021). High-pressure serpentinization and abiotic methane formation in metaperidotite from the Appalachian subduction, northern Vermont. Lithos, 396–397, 106190.

Cannaò, E., and Malaspina, N. (2018). From oceanic to continental subduction: Implications for the geochemical and redox evolution of the supra-subduction mantle. Geosphere, 14, 2311–2336.

Caurant, C., Debret, B., Ménez, B., Nicollet, C., and Bouilhol, P. (2023). Redox heterogeneities in a subducting slab: Example from the Monviso meta-ophiolite (Western Alps, Italy). Lithos, 446, 107136.

Connolly, J. A. D. (1990). Multivariable phase-diagrams - an algorithm based on generalized thermodynamics. American Journal of Science, 290, 666–718.

Connolly, J. A. D. (1995). Phase diagram methods for graphitic rocks and application to the system C–O–H–FeO–TiO_2–SiO_2. Contributions to Mineralogy and Petrology, 119, 94–116.

Connolly, J. A. D. (2005). Computation of phase equilibria by linear programming: a tool for geodynamic modeling and its application to subduction zone decarbonation. Earth and Planetary Science Letters, 236, 524–541.

Debret, B., Sverjensky, D. A. (2017). Highly oxidising fluids generated during serpentinite breakdown in subduction zones. Scientific reports, 7, 10351.

Demouchy, S., Bolfan-Casanova, N. (2016). Distribution and transport of hydrogen in the lithospheric mantle: A review. Lithos, 240, 402–425.

Dersch, O. and Rauch, F. (1999). Water uptake of quartz investigated by means of ion-beam analysis. Fresenius' journal of analytical chemistry, 365, 114–116.

Doremus R. H. (1995). Diffusion of water in silica glass. Journal of Materials Research. 10, 2379–2389.

Efimchenko, V. S., Fedotov, V. K., Kuzovnikov, M. A., Zhuravlev, A. S., and Bulychev, B. M. (2013). Hydrogen solubility in amorphous silica at pressures up to 75 kbar. The Journal of Physical Chemistry B, 117, 422–425.

Efimchenko, V. S., Fedotov, V. K., Kuzovnikov, M. A., Meletov, K. P., and Bulychev, B. M. (2014). Hydrogen solubility in cristobalite at high pressure. The Journal of Physical Chemistry A, 118, 10268–10272.

Eugster, H. P. (1957). Heterogeneous reactions involving oxidation and reduction at high pressures and temperatures. The Journal of Chemical Physics, 26, 1760–1761.

Eugster, H. P., and Skippen, G. B. (1967). Igneous and metamorphic reactions involving gas equilibria. Researches in Geochemistry, 2, 492–520.

Eugster, H. P., and Wones, D. R. (1962). Stability Relations of the ferruginous biotite, annite, Journal of Petrology 3, 82–125.

Evans, K. A., Powell, R., and Frost, B. R. (2013). Using equilibrium thermodynamics in the study of metasomatic alteration, illustrated by an application to serpentinites. Lithos, 168, 67–84.

Evans, K. A., Reddy, S. M., Tomkins, A. G., Crossley, R. J., and Frost, B. R. (2017). Effects of geodynamic setting on the redox state of fluids released by subducted mantle lithosphere. Lithos, 278, 26–42.

Fegley, B., 2013. Practical chemical thermodynamics for geoscientists. Academic Press.

Fei, Y., and Bertka, C. M. (1999). Phase transitions in the Earth's mantle and mantle mineralogy. In: Fei, Y., Bertka, C. M., Mysen B. O. (Eds.) Mantle Petrology: Field Observations and High-Pressure Experimentation; A Tribute to F. R. Boyd, Geochemical Society, Washington, DC, 189–207, Spec. Publ.

Feng, L., Shen, Y., Wu, T., Liu, B., Zhang, D. and Tang, Z. (2020). Adsorption equilibrium isotherms and thermodynamic analysis of CH_4, CO_2, CO, N_2 and H_2 on NaY Zeolite. Adsorption, 26, 1101–1111.

Figowy, S., Mohn, C. E., and Caracas, R. (2024). Noble gas migration in silica polymorphs at Earth's mantle conditions. Earth and Planetary Science Letters, 633, 118637.

Foley, S. F. (2011). A reappraisal of redox melting in the Earth's mantle as a function of tectonic setting and time. Journal of Petrology, 52, 1363–1391.

Fumagalli, P. and Poli, S. (2005). Experimentally determined phase relations in hydrous peridotites to 6.5 GPa and their consequences on the dynamics of subduction zones. Journal of Petrology, 46, 555–578.

Futera, Z., Yong, X., Pan, Y., John, S. T. and English, N. J. (2017). Formation and properties of water from quartz and hydrogen at high pressure and temperature. Earth and Planetary Science Letters, 461, 54–60.

Giuntoli, F., Vitale Brovarone, A., and Menegon, L. (2020). Feedback between high-pressure genesis of abiotic methane and strain localization in subducted carbonate rocks. Scientific Reports, 10, 9848.

Giuntoli, F., Menegon, L., Siron, G., Cognigni, F., Leroux, H., Compagnoni, R., Rossi, M. and Vitale Brovarone, A. (2024). Methane-hydrogen-rich fluid migration may trigger seismic failure in subduction zones at forearc depths. Nature Communications, 15, 480.

Hirschmann, M. M., Withers, A. C., Ardia, P., and Foley, N. T. (2012). Solubility of molecular hydrogen in silicate melts and consequences for volatile evolution of terrestrial planets. Earth and Planetary Science Letters, 345, 38–48.

Hirschmann, M. M. (2021). Iron-wüstite revisited: a revised calibration accounting for variable stoichiometry and the effects of pressure. Geochimica et Cosmochimica Acta, 313, 74–84.

Holland, T. J. B. and Powell, R. (2011). An improved and extended internally consistent thermodynamic dataset for phases of petrological interest, involving a new equation of state for solids. Journal of Metamorphic Geology, 29, 333–383.

Holloway, J. R. (1977). Fugacity and activity of molecular species in supercritical fluids. In: Frase,r D. (Ed.) Thermodynamics in geology, Reidel, Boston, 161–181

Karato, S. (2006). Influence of hydrogen-related defects on the electrical conductivity and plastic deformation of mantle minerals: a critical review. In: Jacobsen, S. D., van der Lee, S. (Eds.), Earth's Deep Water Cycle. American Geophysical Union, Washington DC, 113–129

Kasting, J. F., Eggler, D. H., and Raeburn, S. P. (1993). Mantle redox evolution and the oxidation state of the Archean atmosphere. The Journal of geology, 101, 245–257.

Keppler, H., Ohtani. E., and Yang, X. (2024). The subduction of hydrogen: deep water cycling, induced seismicity, and plate tectonics. Elements 20, 229–234.

Malaspina, N., Langenhorst, F., Tumiati, S., Campione, M., Frezzotti, M. L., and Poli, S. (2017). The redox budget of crust-derived fluid phases at the slab-mantle interface. Geochimica et Cosmochimica Acta, 209, 70–84.

Malaspina, N., Campione, M., Tumiati, S., Murri, M., Fumagalli, P., Cerantola, V., La Fortezza, M. and Scambelluri, M. (2023). Epitactic magnetite growth in fluid inclusions as driving force for olivine oxidation coupled with hydrogen production at high pressure. Chemical Geology, 629, 121495.

Matjuschkin, V., Brooker, R. A., Tattitch, B., Blundy, J. D. and Stamper, C. C. (2015). Control and monitoring of oxygen fugacity in piston cylinder experiments. Contributions to Mineralogy and Petrology, 169, 9.

Manning, C. E. (2004). The chemistry of subduction-zone fluids. Earth and Planetary Science Letters, 223, 1–16.

Merdith, A. S., Daniel, I., Sverjensky, D., Andreani, M., Mather, B., Williams, S., and Vitale Brovarone, A. (2023). Global hydrogen production during high-pressure serpentinization of subducting slabs. Geochemistry, Geophysics, Geosystems, 24, e2023GC010947.

Miozzi, F., and Tumiati, S. (2020). Aqueous concentration of CO_2 in carbon-saturated fluids asa highly sensitive oxybarometer. Geochemical Perspective Letters, 16, 30–34.

Moine, B. N., Bolfan-Casanova, N., Radu, I. B., Ionov, D. A., Costin, G., Korsakov, A. V., Golovin, A. V., Oleinikov, O. B., Deloule, E. and Cottin, J. Y. (2020). Molecular hydrogen in minerals as a clue to interpret ∂D variations in the mantle. Nature Communications, 11, 3604.

Myers, A. L. (2002). Thermodynamics of adsorption in porous materials. AIChE journal, 48, 145–160.

Ohtani, E. (2021). Hydration and dehydration in Earth's interior. Annual Review of Earth and Planetary Sciences, 49, 253–278.

O'Neill, H. S. C., and Pownceby, M. I. (1993) Thermodynamic data from redox reactions at high temperatures. I. An experimental and theoretical assessment of the electrochemical method using stabilized zirconia electrolytes, with revised values for the Fe-"FeO", Co-CoO, Ni-NiO and Cu-Cu_2O oxygen buffers, and new data for the W-WO_2 buffer. Contributions to Mineralogy and Petrology, 114, 296–314.

Peng, W., Zhang, L., Tumiati, S., Brovarone, A. V., Hu, H., Cai, Y., and Shen, T. (2021). Abiotic methane generation through reduction of serpentinite-hosted dolomite: implications for carbon mobility in subduction zones. Geochimica et Cosmochimica Acta, 311, 119–140.

Peng, W., Tumiati, S., Zhang, L., Tiraboschi, C., Vitale Brovarone, A., Toffolo, L., and Poli, S. (2022). An experimental study on kinetics-controlled Ca-carbonate aqueous reduction into CH_4 (1 and 2 GPa, 550 C): Implications for C mobility in subduction zones. Journal of Petrology, 63, egac070.

Pitzer, K. S. and Sterner, S. M. (1994). Equations of state valid continuously from zero to extreme pressures for H_2O and CO_2. The Journal of chemical physics, 101, 3111–3116.

Poli, S., Franzolin, E., Fumagalli, P., and Crottini, A. (2009). The transport of carbon and hydrogen in subducted oceanic crust: An experimental study to 5 GPa. Earth and Planetary Science Letters, 278, 350–360.

Regenauer-Lieb, K., Yuen, D. A., & Branlund, J. (2001). The initiation of subduction: criticality by addition of water? Science, 294, 578–580.

Robie, R. A., and Hemingway, B. S. (1995). Thermodynamic properties of minerals and related substances at 298.15 K and 1 bar (105 Pascals) pressure and at higher temperatures. U.S. Geological Survey Bulletin. 2131, 461.

Sato, T., Funamori, N., and Yagi, T. (2011). Helium penetrates into silica glass and reduces its compressibility. Nature Communications, 2, 345.

Shaw, H. R. (1963). Hydrogen-water vapor mixtures: Control of hydrothermal atmospheres by hydrogen osmosis. Science, 139, 1220–1222.

Schmidt, M. W and Poli, S. (2014) Devolatilization during subduction. In: Holland, H. D., Turekian, K. K. and Rudnick, R. L., (Eds.), Treatise on Geochemistry 2nd Edition – The Crust. Elsevier/Pergamon, Amsterdam, 669–701.

Shinozaki, A., Hirai, H., Kagi, H., Kondo, T., Okada, T., Nishio-Hamane, D., Machida, S.I., Irifune, T., Kikegawa, T. and Yagi, T. (2012). Reaction of forsterite with hydrogen molecules at high pressure and temperature. Physics and Chemistry of Minerals, 39, 123–129.

Stachel, T., and Luth, R. W. (2015). Diamond formation–Where, when and how?. Lithos, 220, 200–220.

Stalder, R. (2021). OH point defects in quartz–a review. European Journal of Mineralogy, 33, 145–163.

Syracuse, E. M., van Keken, P. E., and Abers, G. A. (2010). The global range of subduction zone thermal models. Physics of the Earth and Planetary Interiors, 183, 73–90.

Tedds, S., Walton, A., Broom, D. P., and Book, D. (2011). Characterisation of porous hydrogen storage materials: carbons, zeolites, MOFs and PIMs. Faraday discussions, 151, 75–94.

Tiraboschi, C., Tumiati, S., Recchia, S., Miozzi, F. and Poli, S. (2016). Quantitative analysis of COH fluids synthesized at HP–HT conditions: an optimized methodology to measure volatiles in experimental capsules. Geofluids, 16, 841–855.

Toffolo L., Tumiati S., Villa A., Fumagalli P., Amalfa A., and Miozzi F. (2023). Experimental dissolution of carbonaceous materials in water at 1 GPa and 550 °C: Assessing the role of carbon forms and redox state on COH fluid production and composition during forearc subduction of organic matter. Frontiers in Earth Science, 11:1013014.

Toffolo, L., Minopoli, L., Ferrari, E., and Tumiati, S. (2025). A reliable analytical procedure to determine the carbon isotopic signature of CO_2-bearing COH fluids generated in petrological experiments. European Journal of Mineralogy, 37, 25–37.

Toffolo, L., Tumiati, S., Confortini, G., Gatta, D. G., Poli, S., Bouvier, A. S., and Fumagalli, P. (2026). QMS dataset and data processing routine. Dataset and software. figshare. 10.6084/m9.figshare.34923636 .

Tumiati, S., Tiraboschi, C., Sverjensky, D. A., Pettke, T., Recchia, S., Ulmer, P., Miozzi, F. and Poli, S., 2017. Silicate dissolution boosts the CO_2 concentrations in subduction fluids. Nature Communications, 8, 616.

Tumiati, S., Tiraboschi, C., Miozzi, F., Vitale Brovarone, A., Manning, C. E., Sverjensky, D. A., Milani, S., and Poli, S. (2020). Dissolution susceptibility of glass-like carbon versus crystalline graphite in high-pressure aqueous fluids and implications for the behavior of organic matter in subduction zones. Geochimica et Cosmochimica Acta, 273, 383–402.

Tumiati, S., Recchia, S., Remusat, L., Tiraboschi, C., Sverjensky, D. A., Manning, C. E., Vitale Brovarone, A., Boutier, A., Spanu, D. and Poli, S., 2022. Subducted organic matter buffered by marine carbonate rules the carbon isotopic signature of arc emissions. Nature Communications, 13, 2909.

Vitale Brovarone, A., Martinez, I., Elmaleh, A., Compagnoni, R., Chaduteau, C., Ferraris, C., and Esteve, I. (2017). Massive production of abiotic methane during subduction evidenced in metamorphosed ophicarbonates from the Italian Alps. Nature Communications, 8, 14134.

Vitale Brovarone, A., Thomassot, E., Tumiati, S., Siron, G., Consuma, G., Alpermann, T., Ague, J. J., Nestola, F., Giovannelli, D., Sverjensky, D. A. and Toffolo, L. (2026). Unconventional water and hydrous mineral formation from dry minerals and H_2 fluids. Science Advances, 12, p.eaee6559.

884 Walker, D., Carpenter, M. A., and Hitch, C. M. (1990). Some simplifications to multianvil devices
885 for high pressure experiments. American Mineralogist, 75, 1020–1028.

886 Yang, X., Keppler, H., and Li, Y. (2016). Molecular hydrogen in mantle minerals. Geochemical
887 Perspectives Letters, 2, 160–168.

888 Yaremov, P. S., and Il'in, V. G. (2008). Features of the adsorption of hydrogen by various types of
889 microporous materials. Theoretical and Experimental Chemistry, 44, 67–74.

Supplementary Files

This is a list of supplementary files associated with this preprint. Click to download.

- SupportingInformation41126NatComm.docx